Cryptomare Delineations using Craters as Probes to Lunar Stratigraphy: Use of Multispectral Clementine Data as a Tool; I. Antonenko, J. W. Head, C. M. Pieters. Dept. Geol., Brown Univ., Providence, RI 02912 USA, irene_antonenko@brown.edu.

Hidden mare deposits, or cryptomare, present evidence of ancient mare volcanism [1], and thus merit further study. We have addressed issues of cryptomare identification [2], and presented techniques for determining cryptomare geometry using dark halo impact craters (DHCs) which punch through overlying ejecta to excavate underlying mare material [3]. These techniques have been applied to a study area on the western limb of the Moon, using rectified Earth-based telescopic images and Zond data. The resolution and coverage of these data sets, however, is fairly limiting. Furthermore, visual identification of DHCs requires that the soils developed on the crater ejecta be spectrally mature. The Clementine data set, with global coverage, improved resolution, and multiple channels, presents a new opportunity to expand our studies, allowing smaller and less mature craters to be considered.

As a test area, we chose a region of light plains in Schickard crater on the western limb of the Moon (Fig. 1). This area exhibits a variety of features including a large subdued crater, a dark halo crater in the south-west surrounded by a region of smooth, low albedo ejecta, and a large number of small, fresh craters. We prepared a Clementine frame of this area, working with 5 UVVIS bands, calibrating and registering the data as described in [4] to produce a single image cube. Ratios of the 415nm, 750nm, and 950nm filters were then obtained [4]. Figs 2 and 3 show 415/750nm and 750/950nm ratio images respectively, contrast stretched to show the highs (the checkered pattern in Fig 3 is an artifact of the compression algorithm this data was subjected to before transmission to Earth).

We are interested first in identifying the presence of a mafic component within the craters in our image, and second in determining whether it is basaltic in composition. The first part can be accomplished by comparing the 415/750nm and 750/950nm ratio images. The 415/750nm ratio measures the continuum slope steepness in the visible. Bright areas in Fig 2 represent flatter continuum slopes which generally indicate fresh or feldspathic materials. The 750/950nm ratio is an approximate measure of the strength of the ferrous absorption feature near 1μm. Bright areas in Fig 3 represent strong absorption features, indicating the presence of abundant mafic minerals or fresh materials [5]. Areas which are bright in Fig 3 but not in Fig 2 represent a strong absorption feature produced by iron bearing minerals and thus indicate a mafic component. Looking at Figs 2 and 3, we can see that the dark halo crater has a strong mafic component, many of the small craters in the north-west also have a strong mafic component, and surprisingly, only a portion of the wall of the large subdued crater appears to have a strong mafic component.

Our analysis can be extended by considering 5-channel spectra taken from key areas in the image. We collected average 3X3 pixel spectra for the locations shown in Fig 1. Representative spectra of fresh materials, gathered from the slopes of various small craters and in a traverse around the slopes of the large degraded crater, are shown in Fig 4. Craters whose spectra exhibit a ferrous absorption feature near 1 μm are interpreted as tapping high-Ca pyroxene-rich material indicating buried basalt (Fig 4A). Those that exhibit a shorter wavelength absorption or a very weak absorption are interpreted as tapping primarily highland material (Fig 4B). The combined analysis of spectra and ratio figures indicates that craters on the western side of the image tap into buried basalt and that the large subdued crater impacted the edge of this cryptomare deposit.

We used the spatial distribution of craters that exhibit basaltic properties to estimate the cryptomare boundary in this area. In Fig 5, we present a sketch map of the cryptomare extent for this frame. Areas where crater spectra indicate basaltic compositions (indicated by solid squares) are designated as cryptomare regions, areas where crater spectra indicate highland material (open squares) we designated non-cryptomare regions, areas where craters have ambiguous spectra, neither strongly mafic nor strongly feldspathic (half-filled squares), are marked as ambiguous. Confirmation of the estimated boundaries of large scale cryptomare deposits will be evaluated with analysis of independent contiguous frame sets.

Results of the spectral analysis can also be used to estimate the depth of the cryptomare deposit. The presence of basaltic material on the slopes of even the smallest craters in the north-west corner of the image (0.5 km in diameter) suggest the obscuring layer here is very thin, <50 m [3]. The largest crater exhibiting spectra with consistent basaltic characteristics is the dark halo crater in the south-west corner of the image. This 4.7 km diameter crater excavates basaltic material from a depth of approximately 500 m [3]. Thus, the cryptomare in this region must be at least 450 m thick.

The improved resolution and multispectral nature of the Clementine data set allows us to expand the repertoire of techniques available for determination of cryptomare characteristics. Spectral analysis can be used to determine the basaltic nature of fresh material on crater slopes. Analysis of these small, fresh craters can be used to delineate cryptomare boundaries.

Identification of basaltic materials in the smallest craters can help to constrain the thickness of the obscuring layer, thus improving overall cryptomare thickness estimates.

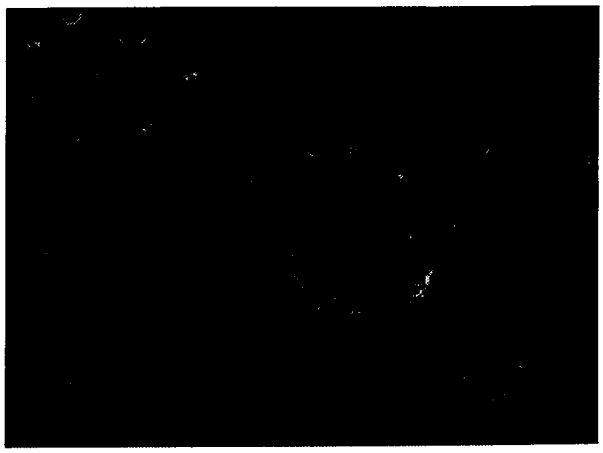

Figure 1: Blue 750 nm filter Clementine image of the test area, showing the locations of spot spectra.

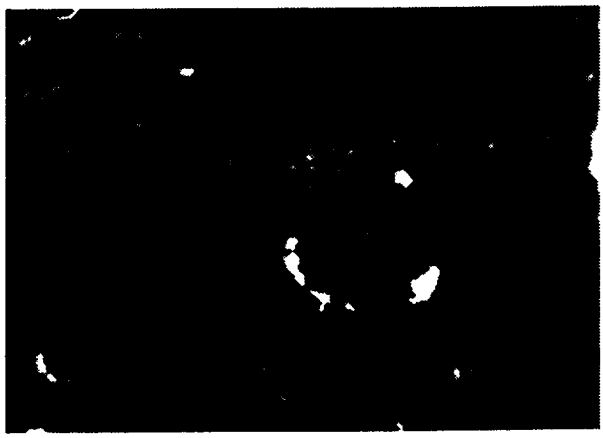

Figure 2: 415/750 nm ratio image of the test area.

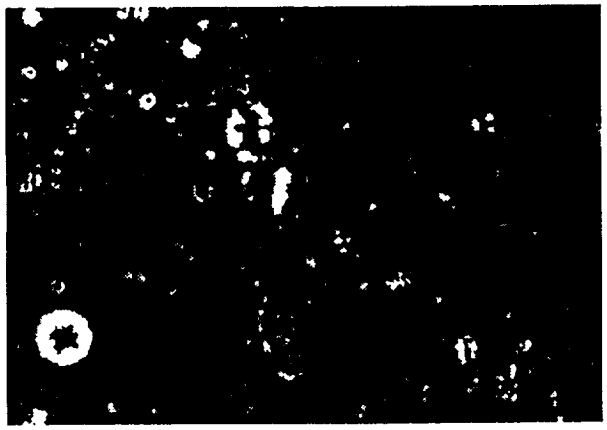

Figure 3: 750/950 nm ratio image of the test area.

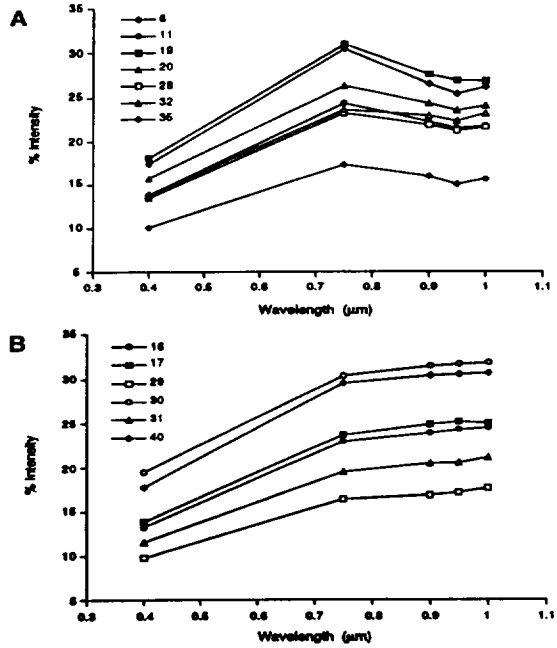

Figure 4: Representative spectra of fresh materials interpreted as indicating basalts and highland material B. Spectra locations are shown in Fig 1.

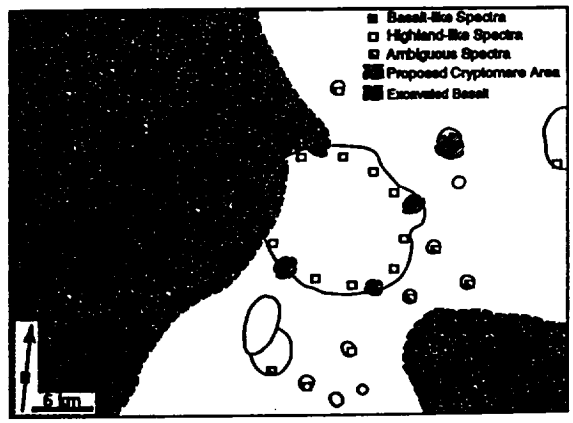

Figure 5: Sketch map of area, showing cryptomare boundaries and location of isolated patches of excavated basalt, determined from spectra and ratio images

References: [1] P. Schultz & P. Spudis, *PLPSC* 10, 2899, 1979; J. Bell & B. Hawke, *PLPSC* 12, 665, 1981. [2] I. Antonenko *et al.*, *EMP*, 69,141,1995. [3] I. Antonenko & J. Head, *LPSC* 25, 35, 1994; I. Antonenko & J. Head, *LPSC* 26, 47, 1995; I. Antonenko and J.W. Head, in preparation. [4] C.M. Pieters *et al.*, *Science* , 266, 1844, 1994; C.M. Pieters *et al.*, http//:www.planetary.brown.edu/clementine/calibration.html, 1996. [5] E.M. Fischer and C.M. Pieters, *Icarus*, 1995; J.B. Adams and T.B. McCord, *Science*, 171, 567, 1971; C.M. Pieters *et al.*, *JGR*, E98, 17127, 1993.

Results of Experimental Dark Halo Crater Studies: Implications for Lunar Cryptomare Thickness Measurements; I. Antonenko,[1] M.J. Cintala[2], J.W. Head,[1] F. Hörz[2]. [1]Dept. Geol. Sci., Brown Univ., Providence, RI 02912 USA; [2]Code SN4, NASA Johnson Space Center, Houston, TX 77058 USA.

Summary: Our desire to study cryptomaria through analysis of dark-halo craters has prompted an experimental program to refine our understanding of the conditions of their formation. To this end, a series of impacts into layered sand targets was performed to determine mare (d_m) and highland substrate (d_h) penetration required to form or obscure a dark halo. Analysis of the results yields the relations $d_m = 0.21 d_e$ and $d_h \geq 0.34 d_e$ where d_e is the depth of excavation. Caution must be used in applying these values, since our target materials do not simulate the spectral characteristics of the Moon.

Background: Dark halo impact craters (DHC's) provide evidence for buried mare materials [1,2] and, under suitable conditions, can be used to estimate the thicknesses of such cryptomare deposits. In any given area, the smallest observed DHC should define the top of the cryptomare, and therefore the thickness of the overlying, obscuring ejecta, while the largest observed DHC should define a minimum estimate of the bottom of the mare layer. The difference between the mare base and the overlying ejecta provides an estimate of the cryptomare thickness [3].

The determination of these thicknesses, however, is a complex process (Fig. 1 and 2). First the depth of the transient crater (d_T) must be obtained. This can be determined by measuring the rim-to-rim diameter of the crater (D_T), then converting this diameter to the transient rim-to-rim diameter (D_{tc}) and the transient rim-to-floor depth (d_T) [4]. From this value, the depth of excavation (d_e) from the pre-impact surface is determined using the relation $d_e = 0.33 d_T$ [5], giving a first order approximation of the thickness of the overlying deposits. This approach has been applied to our study area on the western limb of the Moon, where the d_e values of minimum DHC's were found to be generally consistent with theoretical predictions [6] for ejecta from Orientale, and cryptomare thicknesses were estimated to be on average 900 m [7].

Another factor, however, must be considered. Figure 1 illustrates how some penetration into the mare layer (d_m) is required before a dark halo becomes visible. This value d_m will affect estimates of the ejecta thickness for the smallest DHC's. Similarly, some penetration into the highland substrate (d_h)is required before sufficient highland material is ejected to obscure a dark halo. This value d_h will affect estimates of mare depth for the largest DHC's, assuming they are tapping the bottom of the cryptomare. The magnitude of these two values is not known. We therefore began a series of experiments to simulate dark halo formation, in order to determine the values of d_m and d_h.

Experiments: Layered targets of dyed, resin-coated sand were prepared to simulate lunar stratigraphy. These targets were impacted at velocities of 1, 1.5 and 2 km/s, using spherical projectiles, 6.35 mm in diameter; most projectiles were glass, but aluminum and nylon spheres were also used. After the impact event, the targets were baked to solidify them and then sawed in half, allowing for accurate measurements of subsurface features(Fig. 2).

The experiments were conducted in three phases. In the first phase, a light-colored layer over a dark layer was used to study the formation of simple, dark halos. The thickness of the light top layer was varied for each velocity until the underlying dark layer was excavated in sufficient quantities to produce a barely visible dark halo. A barely visible DHC was defined by the presence of a tenuous, but relatively symmetrical, halo of material from the dark layer around the experimental crater, identified by visual inspection. Spectral measurements of some of the craters were also taken, using the portable spectrometer MINI. These measurements show that, the definitions of spectral and visible detectability coincide in these experiments[8].

In the second phase, we simulated dark halo obscuration by impacting targets in which a layer of dark material was sandwiched between two layers of light material. The thicknesses of the top light layer and the dark layer were varied in order to permit ejection of sufficient quantities of the lower light layer to obscure the dark halo. Only glass projectiles were used in this series. Physical constraints on the maximum size of the crater we could produce and the minimum layer thickness that could be constructed prevented us from completely obscuring the dark halo.

In the third phase, we attempted to improve our analogy to the Moon by replacing the top light layer with a layer of mixed light and dark material. The thickness of this mixed layer was then varied until the underlying pure dark layer was excavated in sufficient quantities to produce a visible DHC. Again, the presence of a DHC was identified by visual inspection, and only glass projectiles were used.

Results: We identified three different types of craters in phase 1; DHC's with well-developed symmetrical halos of dark material, minimum DHC's with tenuous dark halos, and incipient DHC's with no visible halo but emergent excavation of dark material. The ratio of the top layer thickness divided by the crater

depth (t/d_r) is plotted in Fig. 3 for these craters as a function of crater type and projectile. As expected, incipient craters generally have higher t/d_r ratios, DHC's have lower t/d_r ratios, and minimum DHC's have intermediate ratios. Trends apparently due to projectile density can be seen, with the denser aluminum producing generally higher t/d_r ratios and lighter nylon lower ratios relative to the glass projectiles.

For Incipient DHC's, the t/d_r ratio represents the excavation depth/depth (d_e/d_r). Taking an average of this ratio for all Incipient DHC's produced by glass projectiles gives a value of 0.324, very close to the value of 0.33 from [5]. Thus we can be confident in our assessments. Taking the average for all glass produced Minimum DHC's gives layer thickness/crater depth (t/d_r) to be 0.255 ($t \approx 0.26 d_r$). Considering that $d_m = d_e - t$, we can see that $d_m = 0.07 d_r$ or $d_m = 0.21 d_e$, for glass projectiles. Variations in projectile density may affect these values by no more than ±5%. Variations in velocity may also have a small affect on these values at the velocity range we considered.

As was mentioned above, we did not achieve a complete obscuration of a dark halo in phase 2 of our experiments. However, we did observe four craters with distinct light halos. These can provide a lower bound for the value of d_h. The average t/d_r value for these craters is 0.216. By analogy with d_m we calculate that $d_h = 0.11 d_r$ or $d_h = 0.34 d_e$ at the very least.

The results of our phase 3 experiments showed only incipient and minimum DHC's. For incipient DHC's, a thickness of less than d_e was found for top layers with more than a 10% dark component in the mixture. This is most likely due to the difficulty of identifying a small number of excavated dark grains on a background that itself contains dark material. Only 3 minimum DHC's were produced in this phase. The value of d_m appears to vary a little in response to the composition of the top layer, however, more work is needed before these findings can be confirmed.

Application: Our experiments show that d_m and d_h are very important parameters to consider when applying this technique to estimates of cryptomare thicknesses. When the results of this experimentation are applied to our study area on the western limb of the Moon, the resulting average cryptomare thickness is found to be 550m, a decrease of 39% from our original 900m estimate. It must be noted, however, that our experimental conditions were not intended to simulate the spectral properties of the Moon. The albedo contrast and grain size-to-crater ratio of our materials is much greater, potentially affecting the detection threshold of our DHC's and thus the value of d_m and d_h [8]. Further work is needed to resolve the extent of such an effect.

References: [1] P. Schultz & P. Spudis, *PLPSC* 10, 2899, 1979; J. Bell & B. Hawke, *PLPSC* 12, 665, 1981. [2] I. Antonenko *et al.*, *EMP*, 69,141,1995. [3] I. Antonenko & J. Head, *LPSC* 25, 35, 1994; I. Antonenko & J. Head, *LPSC* 26, 47, 1995. [4] J.H. Melosh *Impact Cratering: A Geologic Process*, 1989. [5] D. Stöffler *et al.*, *JGR*, 80, 4062, 1975. [6] T. McGetchin *et al.*, *EPSL*, 20, 226,1973; P. Schultz *et al.*, *PLPSC* 12, 181, 1981. [7] Antonenko and Head, *in preparation*. [8] I. Antonenko *et al.*, *LPSC* 27, 31, 1995.

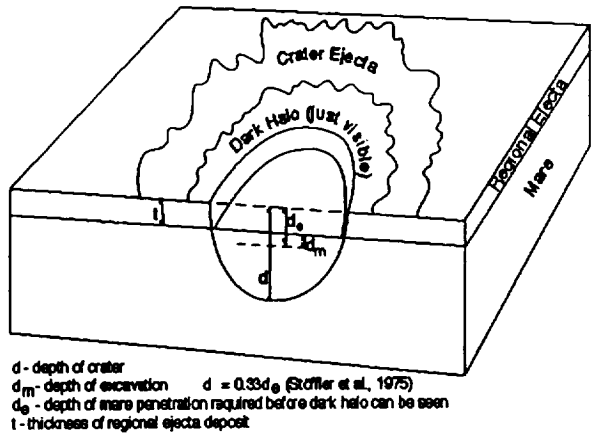

Fig. 1. Block diagram showing the relationship between crater depth (d), depth of excavation (d_e) and depth of mare penetration (d_m) for a minimum DHC.

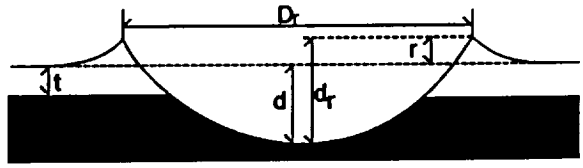

Fig. 2. Diagram illustrating the relationship between the measured variables for our experiments.

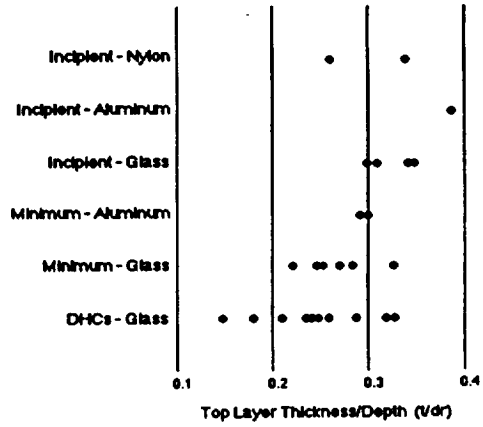

Fig. 3. Plot of the top layer thickness divided by the crater depth (t/d_r) for simple, dark-halo craters as a function of crater type and projectile composition.

HOT SPOTS ON EARTH, VENUS, AND MARS: SPHERICAL HARMONIC SPECTRA

L. S. Crumpler[1] and *Justin Revenaugh*[2]; *(1) New Mexico Museum of Natural History and Science, 1801 Mountain Rd NW, Albuquerque, NM 87104; (2) Department of Earth Sciences, University of California, Santa Cruz, CA 95064*

INTRODUCTION. The distribution of large intraplate magmatic centers is now known for the three largest terrestrial planets [18]. Significant differences in the global geologic characteristics of Earth, Venus, and Mars were anticipated prior to these new observations [1] based on their different global hypsometries [2] and potentially different thermal histories [3]. In this study, we assess the spherical harmonic spectra of large magmatic centers on the terrestrial planets and show that, despite the known dissimilarities in global geology and surface ages, Venus, Earth, and Mars share some large-scale similarities in the arrangement of physically large and magmatically productive volcanic centers (hot spots).

CHARACTERISTICS OF HOT SPOT VOLCANISM. Volcanic centers on Venus were identified from geologic interpretation of synthetic aperture radar images returned by the Magellan spacecraft [4]. Global reconnaissance of over 1700 volcanic centers [5], and the results of preliminary mission science reports [6] were used to establish the location of all major volcanic centers on Venus and their relationship to global geologic characteristics. Similar maps of the distribution of volcanic centers and their relation to global geologic characteristics were prepared from existing data for Earth and Mars as discussed below. In view of the differences from planet to planet in morphological characteristics of the major magmatic centers that might be identified as hot spots, it is first necessary to justify the selection of the sets for each planet.

Volcanic and magmatic centers on Venus larger than 100 km in diameter were selected for consideration and analysis as only the largest of these volcanic edifices are likely to represent long-term centers of anomalous melting and repeated eruptions over extended periods of time comparable to that characterizing major centers of volcanism on Earth and Mars.

Large volcanic centers on Earth occurs in two fundamental settings: plate boundary and intraplate. Because plate boundaries associated with mobile tectonics are not present on Venus or Mars, the mapped distribution of "intraplate" or "hot spot" volcanism on Earth (Figure 1B) is considered appropriate for comparison with the distribution of volcanism on Venus and Mars. Some confusion exists about the exact definition of a "hot spot" and the degree to which the definition and identification is to be based on observed surface characteristics (e.g., volcano tracks) or inferred subsurface origins (e.g., plumes). The consensus view of hot spot descriptions were merged with additional geophysical criteriua [7] in order to arrive at a list of hot spots that agreed with previous usage and that could also be supported on the basis of numerical arguments. Apart from their distinctive locations and volumes, hot spot volcanism and plate boundary volcanism differ in a variety of significant physical and petrologic characteristics that facilitate their discrimination at statistically significant levels. One class includes hot spots that are typically characterized by tracks of extinct volcanoes and which are correlated with long-wavelength geoid anomalies (harmonic degree 2-10). This association with low harmonic degree characteristics of the global topographic and gravity fields together with their distinctive petrologic characteristics are interpreted

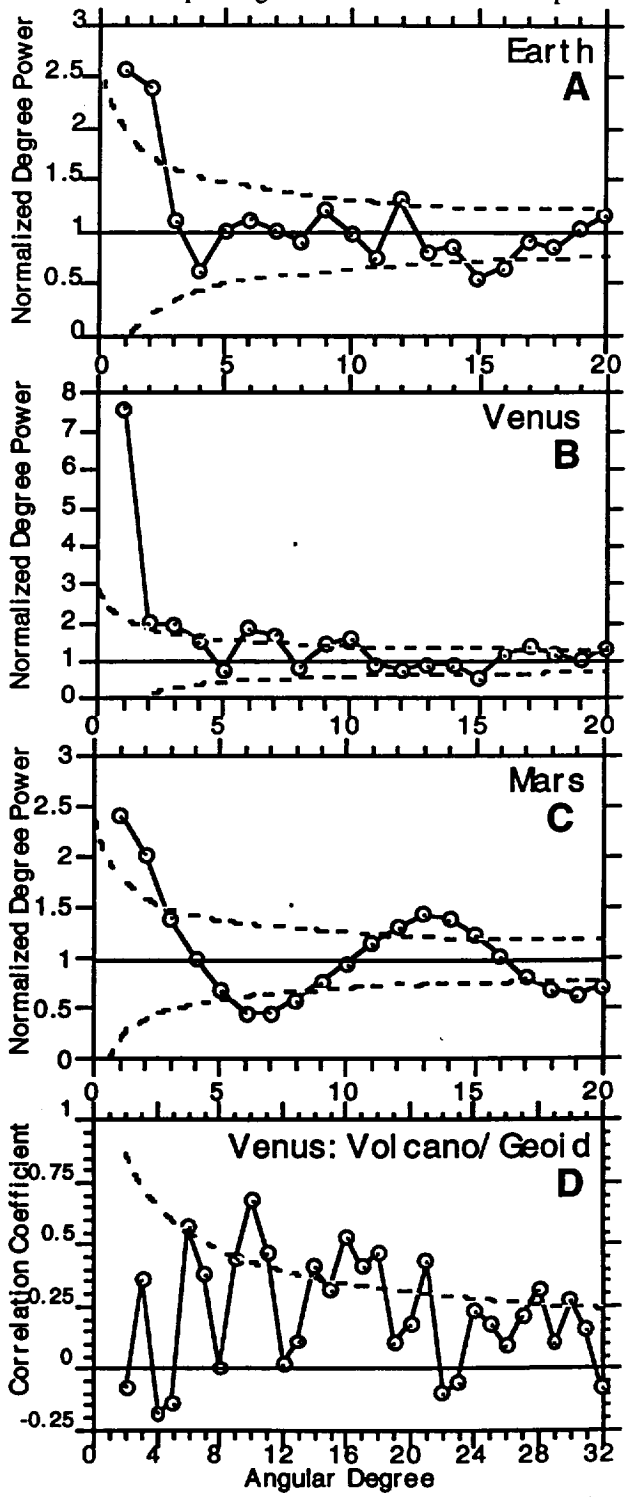

Figure 1. A-C. Harmonic power versus angular degree for hot spots on three terrestrial planets. Dashed line: 95%

confidence limit on uniformity. **D.** Correlation between hotspot distribution and geoid for Venus.

to be a consequence of a sublithospheric and deep-mantle, origin. The list of active hot spots from [8] compiled by Richards et al [9] satisfies most of the criteria determined in Marzoochi and Mulargia's study.

The choice of which volcanic centers to include in a martian hot spot list is much simpler as there are relatively few large volcanoes on Mars, each of which is large by either Venus or Earth standards. Volcanic centers on Mars occur in three settings, the Tharsis region, which is characterized by a hemispheric topographic rise or swell, and is the largest concentration, and the Elysium region and Hellas basin region, both of which occur in the opposite hemisphere.

Finally, consideration must be given to the differences in age of the surfaces of the three planets and corresponding differences in the accumulation period of each population of hot spots. Current estimates for the global surface age of Venus, approximately 500Ma [10], suggest s that the record of volcanism o Venus is comparable to the age of the current hot spot population on Earth [approximately 200 Ma [11]. Thus the total accumulated hot spot population for Earth and Venus are comparable within a factor or two. The time interval recorded in the population of large volcanoes on Mars may be much greater. The oldest volcanoes, those of the Hellas and related highland provinces are estimated at 3.7 to 3.1 Ga [12], whereas the volcanoes of the Tharsis region range from 1.5 to 0.1 Ga [13]. The absolute number of volcanoes on Mars is low and reflects the lower global volume-rate of magma production [14] throughout its geologic history, estimated to be two to three orders of magnitude less than that on Earth or Venus. Although there appears to be a great range in age of volcanism on Mars, the relatively stable surface combined with the declining production rates with time suggest that the population of volcanoes on Mars represents the only cycle of hot spot production on that planet and that mantle events or surface tectonic responsible for the population are not overprinted. Thus there are a variety of reasons for comparing hot spots on Earth with large magmatic centers on Venus and large volcanoes on Mars.

The observed distribution based on this selection has been discussed previously [15]. In general, each planet shows a similar qualitative bipolar arrangement of volcanic centers with three common characteristics: (i) a *primary group*, defined as a significant concentration of volcanic and magmatic centers in which more than one-half of the global population occurs within less than 30% of the global area; (ii) a region peripheral to this concentration in which the regional density is less than or close to that expected for a randomly distributed population, and (iii) a distal region, or *secondary group*, occupying about 30% of the global area in which the density approaches that expected for a globally uniform distribution.

SPHERICAL HARMONIC SPECTRA. For the analysis, each volcano was weighted according to fluxes or volume: For Earth, erosion introduces potential variations, so the estimated fluxes of hot spots [7] were used to establish magnitude data; for Mars, volumes were calculated from existing topographic data; and for Venus, a model for the "average" relief and slope was used based on an extensive survey of large volcano relief and width characteristics [ref]. The spectra for all three planets were then determined out to degree 20. The results (Figure 1) indicate that all three planets are similar in that they are dominated by degrees 1 and/or 2 and have spectra that tend to peak at degree 1 (hemisphericity).

Earth has sub-equal degree 1 and 2 power. This is a combination of the flux high over the Pacific (degree 1), the minor flux high over Africa (degree 2) and the banding about the equator (also degree 2). Venus is dominantly degree 1 with greatest volume within the Beta-Atla-Themis area and lowest volume in the Aphrodite Terra region. Beyond degree 1, the spectrum for Venus is whiter than that of Earth. The hot spot distribution for Mars is similar to Earth in that degrees 1 and 2 dominate. The distribution of volume for Earth differs from a random (uniform) pattern only at degrees 1 and 2. Mars differs at many degrees - the product of clustering which depends strongly on how one constructs the data set. Grouping overlapping or related volcanoes into single units (summing volumes) would result in a whiter, more random spectrum (at high degree). Venus has many degrees that are not random. In terms of the uniformity of hotspot distribution, Mars and Venus differ significantly from Earth. Both Mars and Venus have more energy at high degree, implying less deep-seated (long-wavelength) control over volcanism.

Some insight into the origin of the distribution for Venus may be gained by considering the correlation with geoid. Correlation at high degree is expected since Venus' topography and geoid are strongly correlated at short wavelengths. The highest correlation (degree 10) may be associated with the principal volcanic rises, which are known to have large geoid signatures [16]. If the large concentration in Beta-Atla-Themis is the reflection of a deep upwelling as previously suggested [5], the absence of significant correlation of Venusian volcanoes with geoid at low degrees is evidence that the current hemispheric arrangement is relict and does not reflect currently active processes. This result is consistent with the observations of Grosfils and Head [17] who noted that the large scale patterns of surface strain surrounding the Beta-Atla-Themis concentration was emplaced concurrently with most of the volcanism.

References. [1] Solomon and Head, 1991, *Science* **252**, 252; [2] Masursky et al., 1980, *Jour. Geophys. Res.* **85**, 8232; [3] Schubert et al., 1990, *Jour. Geophys. Res.* **95**, 14105; [4] Head et al., 1992, *Jour. Geophys. Res.* **97**, 13153 ; Crumpler et al., 1993, *Science* **261**, 591; [5] Crumpler et al, 1997, Venus II, in press; [6] Saunders, 1992, *Jour. Geophys. Res.* **97**, 13067; [7] Sleep, 1990, *Jour. Geophys. Res.* **95**, 6715-6736; [8] Crough and Jurdy , 1980, *Earth Planet. Sci.Lett.***48**, 15; Morgan , 1981, The Sea, vol 7, C. Emilaiani, ed, 443; [9] Richards et al., 1988, *Jour. Geophys. Res.* **93**, 7690; [10] Schaber et al., 1992, *Jour. Geophys. Res.* **97**, 13257; [11] Anderson, 1982, *Nature* **297**, 391; [12] Greeley and Guest, 1987, *U.S.Geol;. Surv. Misc. Invest. Map I-1802-B*; Tanaka et al., 1988, *Proc. Lun. Planet. Sci. Conf.* 18, 665; [13] Scott and Tanaka, 1986, *U.S.Geol;. Surv. Misc. Invest. Map I-1802-A*; Tanaka et al., 1988, *Proc. Lun. Planet. Sci. Conf.* **18**, 665; [14] Greeley and Schneid, 1992, *Science* **254**, 996; [15] Crumpler, 1994, *Lunar Planet Sci.XXV*, 303; [16] Smrekar and Phillips, 1991, Earth Planet Sci. Lett **107**, 582; [17] Grosfils and Head , 1994, *Geophys. Res. Lett.* **21**, 701; [18] Crumpler, 1994, *LPSC XXV*, 303; Crumpler et al., 1993, *Science* **261**, 591.

LATE STAGE ACTIVITY OF LARGE VOLCANOES ON VENUS

L. S. Crumpler[1], J. W. Head[2], and J. C. Aubele[1]; (1) New Mexico Museum of Natural History and Science, 1801 Mountain Rd NW, Albuquerque, NM 87104; (2)Department of Geological Sciences, Brown University, Providence, RI 02912

INTRODUCTION. Several distinctive morphologic classes occur among large volcanoes on Venus [1]. Many of these differences are consistent with the details of interaction with surrounding structural patterns, and variations in late stage activity. The presence of large volcanoes is significant in itself, however, because specific conditions in the feeding reservoir must exist in order for a magmatic center to give rise to edifice growth. In this study we review one of those conditions by examining some possible implications of the typical observed relief characteristics of large volcanoes on Venus.

VOLCANO STRATIGRAPHY. Detailed stratigraphy from mapping of individual large volcanoes [2] indicates that a there is a recurring theme in which early eruptions are voluminous and contribute to widespread regional plains development, and late eruptions are increasingly digitate and radiate from a common vent. We interpret these stratigraphic variations as a record of change in style of eruption over the lifetime each magmatic center.

EDIFICE VOLUME DISTRIBUTION. The observed relief characteristics of large volcanoes records the distribution of volume in a "characteristic" eruption during actual construction of the edifice. The observed population of large volcanoes on Venus consist frequently of regular straight-sloped cones [1, 3] of relatively shallow slope. In order to accumulate a cone of this form, the volume added to the surface about the vent from each eruption, or as a long term average, must have a specific distribution given by

$$dV = 2\pi r[f(R)]dr.$$

f(R) is a "shape" function that describes the profile of the volcano with distance r from the vent and is of the form

$$f(R) = k - \gamma r^{\beta}.$$

For a straight cone of unit height, k and ß are unity and γ is the slope. But for more complex profiles, ß may itself be a complex variable. In order to attain the shape of a straight-sloped right cone (Fig. 1A) typical of large volcanoes on Venus, the ideal or "average" volume distribution with distance from the vent for each eruption must therefore be

$$dV/dr = 2\pi(r - \gamma r^2).$$

Most of the volume of a given shield volcano therefore is in the mid flank region, with smaller incremental volumes in the vent region and distal flanks (Fig. 1A). This is a key observation that establishes importance one of the primary conditions of eruption necessary for construction of any edifice: Until "average" shield building flow unit or flow field accumulated during a single eruption begins following this distribution (Fig. 1A) , an edifice does not begin forming.

ERUPTION VOLUME DISTRIBUTION. The mechanism controlling eruptions such that they attain this distribution is the central question. Stochastic variations over time in the length of straight monotonous flows of uniform width and thickness are not sufficient for the generation of straight sloped edifices; variations in the plan shape, thickness, or both, with distance from the vent are required. Volume effusion rate is likely to be the most variable characteristic between eruptions, followed by secular variations in magma chemistry throughout the history of an individual magmatic center. For basaltic magmas the problem therefore reduces to the conditions responsible for variations in volume of flow fields with distance from the source vent in a typical flow or flow field. Several models may be applicable.

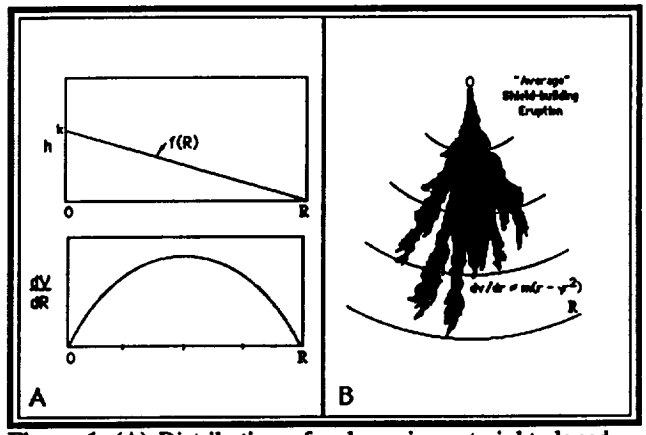

Figure 1. (A) Distribution of volume in a straight-sloped cone. (B) Possible shape of "average" flow field on volcano flank responsible for volume distribution in (A). Concentric arcs represent schematic topographic contours on the flanks of a shield volcano of radius R.

Variations in volume of flow fields with distance from the source vent have been noted from Mt. Etna [4] and have been attributed to variations in effusion rate during the course of a single eruption. The theoretical basis for length/effusion rate relationship has been explored and is related to the dimensionless Grätz number relating the maximum length that flows may attain due to cooling effects [5]. This expression can be recast to estimate the maximum length attainable for flows adding to the accumulation of an individual volcanic edifice for specified effusion rates, slopes, and so on. One consequence of this behavior is that any recurring effusion rate during edifice construction can result in volcanic edifices that are some multiple of the fundamental cooling-limited lava flow length [6].

Recurring effusion rate histories are predicted for eruptions from a shallow reservoir for a variety of reasons. Many eruptions on Earth follow a well-defined effusion rate curve of exponentially decreasing effusion with time [8] which can be related to variations in eruption driving pressures arising from the properties of the magma chamber, the country rock, and the magma rheology. A potential consequence of a changing effusion rate during an eruption was noted by Wadge [4] for Mount Etna: If the effusion rate increases or decreases with time during an eruption, the maximum length of the lava flow produced during that time correspondingly increases and decreases. This behavior can be understood in terms of the *Gz* number and cooling-limited behavior outlined above. Variation in E

cause the critical value of Gz to be attained for different lengths at different times during the eruption; the distribution of lengths accordingly reflects the variations in the shape of the effusion rate curve with time. The process can be expected to be complicated by the tendency for the near-vent flow field to move in well-defined levees or within crusted-over lava tube sections, but the general tendency will be to follow a growth history for individual eruptions similar to that shown in Figure 2.

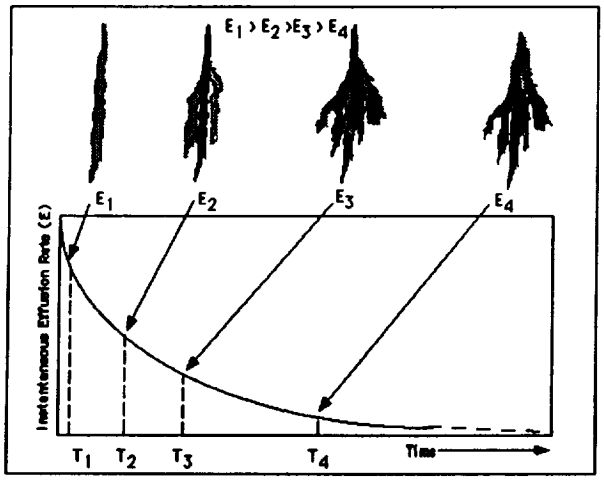

Figure 2. Variation in flow field shape and volume with exponentially declining effusion rate (E) for a single eruption during main phase of shield volcano construction. The gray portions of the field represent flows that are active during the indicated stages (T_1-T_4) of declining effusion.

Two additional ways in which variations in volume distribution may occur include variable arrangements of vents and displacements of the profile associated with central subsidence (including caldera formation) and subsequent edifice re-building. In order for variable arrangements of vents to account for the volume distribution of typical shield volcanoes, the vents must be distributed over the flanks. This can account for the distribution in some volcanoes provided that the vents are distributed in a narrow belt of a particular width for a particular average eruption volume distribution. Such patterns could arise from concentric fissure eruptions, but as a general mechanism, this does not explain the volume distribution in relatively simple edifices. There are few examples of concentric patterns of vents on the large Venus edifices. It is noted that small volcanoes and other evidence for small vents are frequently distributed over a broad region of the summit. This arrangement could arise from the relatively greater predicted depth of reservoirs associated with large volcanoes on Venus [7], owing to the greater dispersal of ascending magmas over the broader area of the underlying reservoir. Depending on the details of the distribution of such vents, the overall low profile and shallow slope of typical large volcanoes on Venus might originate from the correspondingly more distributed volume of accumulated individual eruptions from the edifices.

A premise in all of the above models is that all or most of the observed differences in profile characteristics are a result of variations in the distribution of erupted volumes. The role of intrusive inflation and caldera subsidence in the main edifice during cycles of inflation within the associated shallow magma reservoir may be important in some volcanoes. The magnitude of both inflation and subsidence must be dependent on the depth of the reservoir, and will be particularly influential only in cases where the reservoir resides in either the substrate very near the base of the volcano or within the edifice itself. Although magma reservoirs are commonly located at high levels within the edifice of volcanoes on Earth, and possibly on Mars, the depths to likely reservoirs on Venus [7] are predicted to almost always lie within the substrate. Accordingly, the influence of magma reservoir inflation on large volcano morphometry is predicted to be relatively minor.

From the above discussion, profiles departing from simple straight-sloped cones, in particular those with either steep summits or truncated forms, must represent the results of significant long-term changes or evolution in eruptive behavior of the edifice. Such changes might include late eruption of more differentiated magmas with rheological behaviors that differ from preceding flows, evolution of the magma reservoir such that magma driving pressures and effusion rates undergo long term changes, or structural changes within the volcano itself, perhaps as a result of caldera formation or even inflation of the volcano due to growth of the associated shallow magma reservoir. Detailed observation of the geologic characteristics of all of the individual edifices is necessary in order to determine which of these effects has been influential.

SUMMARY. The building of relatively straight-sloped shield volcanoes is direct evidence for the development of centralized, shallow magma chambers following an earlier, protracted phase of deeply-fed eruptions. Whereas many large volcanoes may initiate as regional effusions of relatively fluid and widespread lavas, the late stage development of shield suggests that centralized reservoirs develop over time

Measurements of the distribution of volume provide some information on the style of eruption during the late phases of edifice coinstruction. Although a variety of mechanisms may operate to distribute the volume in a manner consistent with straight-sloped shields, the variation in effusion during single eruptions is a simple mechanism that can result in the required volume distribution. Late stage activity of large shield volcanoes is evidence for the presence and behavior of shallow magma chambers within the elastic lithosphere operating during the culminating phases of the evolution of each center.

REFERENCES.

[1] Crumpler and others, 1997, (Volcanism chapter), *Venus II*, in press; Crumpler and others, 1993, LPSC XXIV, 365; Head and others, 1992, *LPSC XXIII*, 513;
[2] Keddie and Head, 1994, *Earth Moon Planets* 65, 129-190; Keddie and Head, 1995, *Jour. Geophys. Res.* 100, 11729-11754; [3] Keddie and Head, 1994, *Planet Space Sci* 42, 455-462; [4] Wadge, 1978, *Geology* 6, 503-506; Guest et al., 1987, *Bull. Volcanol.* 49, 527-540; Hughes et al., 1990, Chpt 18 in *Magma Transport & Storage*, M.P.Ryan, ed; [5] Hulme and Fielder, 1977, *Roy. Soc. Phil. Trans* A285, 227-234; Pinkerton and Wilson, 1994, *Bull. Volcanol.* 56, 108-120; [6] Head et al., 1993, LPSC XXIV, 627-628; [7] Head and Wilson, 1992, *Jour. Geophys. Res.* 97, 3877-3903; [8] Wadge, 1981, *J. Volc. Geotherm. Res.* 11, 139-168.

REMOTE AND LOCAL STRESSES AND CALDERAS ON MARS;

L. S. Crumpler[1], J. C. Aubele[1], and J. W. Head[2]; (1)New Mexico Museum of Natural History and Science, 1801 Mountain Rd NW, Albuquerque, NM 87104; (2)Dept. of Geol. Sciences, Brown University, Providence, RI 02912; crumpler@nmmnh.-abq.mus.nm.us

INTRODUCTION. The detailed structure of calderas is a sensitive indicator of the stress environment existing at the time of caldera formation. Unlike regional patterns of strain, such as wrinkle ridges, graben, and fractures, calderas, however, have short time scales for formation and record local stress at essentially point sources. Strain associated with caldera formation and evolution may also be tied stratigraphically to a relatively well-defined geologic unit and well-constrained times. In the following, we have compiled the structural characteristics of calderas on Mars [1] and compared the deduced orientation of remote stress with predicted patterns of global strain, patterns attributable to regional slopes, and patterns attributable to relict or pre-existing substrate structure.

OBSERVATIONS. Several types of structure alignment can be distinguished in the summit calderas of the larger martian volcanoes: (1) overlapping calderas, (2) concentrations of pits and channels on flank sectors, and (3) linear, through-trending fissure patterns. Overlapping and elongated calderas characterize the summits of Olympus Mons and the Tharsis Montes (Figure 1). These patterns are most prominent in larger edifices or the larger calderas that are indicative of large magma reservoirs. Calderas associated with smaller volcanoes, such as Biblis Patera, Ulysses Patera, Ceraunius Tholus, and Albor Tholus are either circular or consist of randomly overlapping caldera segments.

ANALYSIS. Caldera structures preserve regional stress patterns because dikes develop along directions of maximum principal stress. Systematic alignments therefore tend to develop in successive magma reservoirs within an evolving magmatic system [2]. The principles of dike emplacement were reviewed previously [3] and are here briefly re-iterated. A dike is propagated from a magma body, resulting in magma being either erupted at the surface or injected laterally, when the wall failure criteria $P_l + P_m \geq |s_3| + T$ is satisfied [4] and magmatic pressure exceeds the sum of remote stress (minimum compressive stress, s_3) and tensile strength (T) of the country rock. Regional patterns of stress that may influence the orientation of s_3 can arise from strains resulting from either tectonic processes, local and regional relief, or pre-existing, directional variations in the value of T (i.e., pre-existing structural fabrics)[5]. All of these are predicted to have a significant influence on regional stress arrangements on Mars [6,7,8]. The influence of regional topography and its associated stress patterns on dike orientation has been used previously in assessing the orientations of possible dike-related graben sets on Venus [9]. On Mars, basins and basin structures are also likely to be important.

Figure 1 is a comparison of predicted patterns of minimum stress from global topographic relief [8] with orientations of the minimum stress determined from the relevant s_3 indicators (overlapping calderas, concentrations of pits and channels on flank sectors, and linear, through-trending fissure patterns).

DISCUSSION. Calderas are limited in absolute number , so the results of a comparison between observed and predicted patterns are of limited quantitative value. However, logical geologic inferences of regional interest can be made based on observed structure and local/regional associations. The salient points are reviewed in Table 1 which summarizes the principal inferences.

Table 1. Three caldera strain/remote stress associations:

Volcanoes	Timing	Origin of Stress
[AM, PM, AM, Uranius Patera, Hecates, Elysium]	mid-age volcanoes	regional dynamic lithospheric flexural stress
OM, Tharsis Tholus, Ceraunius Tholus	mid and young age	local crustal gravity stress (regional slope and edifice effect)
Tyrrhena, Nili, Meroe, Hadriaca, Peneus, Amphitrites]	old to mid age	regional inheritance from pre-existing structure
[Biblis, Albor, Jovus, Apollonaris, Alba(?)]	old	No (or little) apparent local or regional

Patterns of strain associated with the larger calderas follow stresses predicted from global isostatic flexure patterns [6,7,8] particularly within the large volcanic rises of Tharsis. Notable exceptions in Tharsis include Olympus Mons, Tharsis Tholus, Alba Patera, and Ceraunius Tholus. Fractures obeying the predicted pattern of strain occur around Alba Patera, but do not appear to have operated at the time of magma emplacement. At Olympus Mons, large gravity stresses associated with regional slip of the edifice on the slopes of Tharsis may have dominated the local stress field [9]. This also appears to be the case for Tharsis Tholus.

Patterns of deformation in older calderas may relate to regional and local slope effects. The oldest, and lowest, calderas appear to have been influenced by pre-existing structural fabrics associated with basins.

REFERENCES CITED. [1] Crumpler, et al, 1995, *Lunar Planet. Sci.*, XXVI, 305-306; Crumpler et al., 1994, *Lunar Planet. Sci.* XXV, 305-306; Crumpler, et al, 1995, *Geol. Soc. London Spec. Pub. 110*, 307-347; Crumpler, et al., 1990, *MEVTV Workshop on the Evolution of Magma Bodies on Mars*, Richland, 14-15; [2] Pollard, and Muller, 1976, *Jour. Geophys. Res.* 81, 975-984; Nakamura, 1982, *Bull. Volc.Soc. Japan*, 25, 255-267; [3] Crumpler, Head, and Aubele, 1996, *LPSCXXVII*, 277-278; [4] Gudmundsson, 1988, *J. Volc. Geoth.Res*, 35, 179-194; [5] Nakamura, 1977, *J. Volc. Geotherm. Res.*, 2, 1-16; [6] Banerdt et al., 1982, *Jour. Geophys. Res.*, 87, 9723-97-33; [7] Phillips and Lambeck, 1980, *Rev. Geophys. Sp. Phys.* 18, 27-76; [8] Sleep and Phillips, 1985, *Jour. Geophys. Res.*90,4469-4489; [9] McGovern and Solomon, 1993, *Jour. Geophys. Res.* 98, 23553-23579.

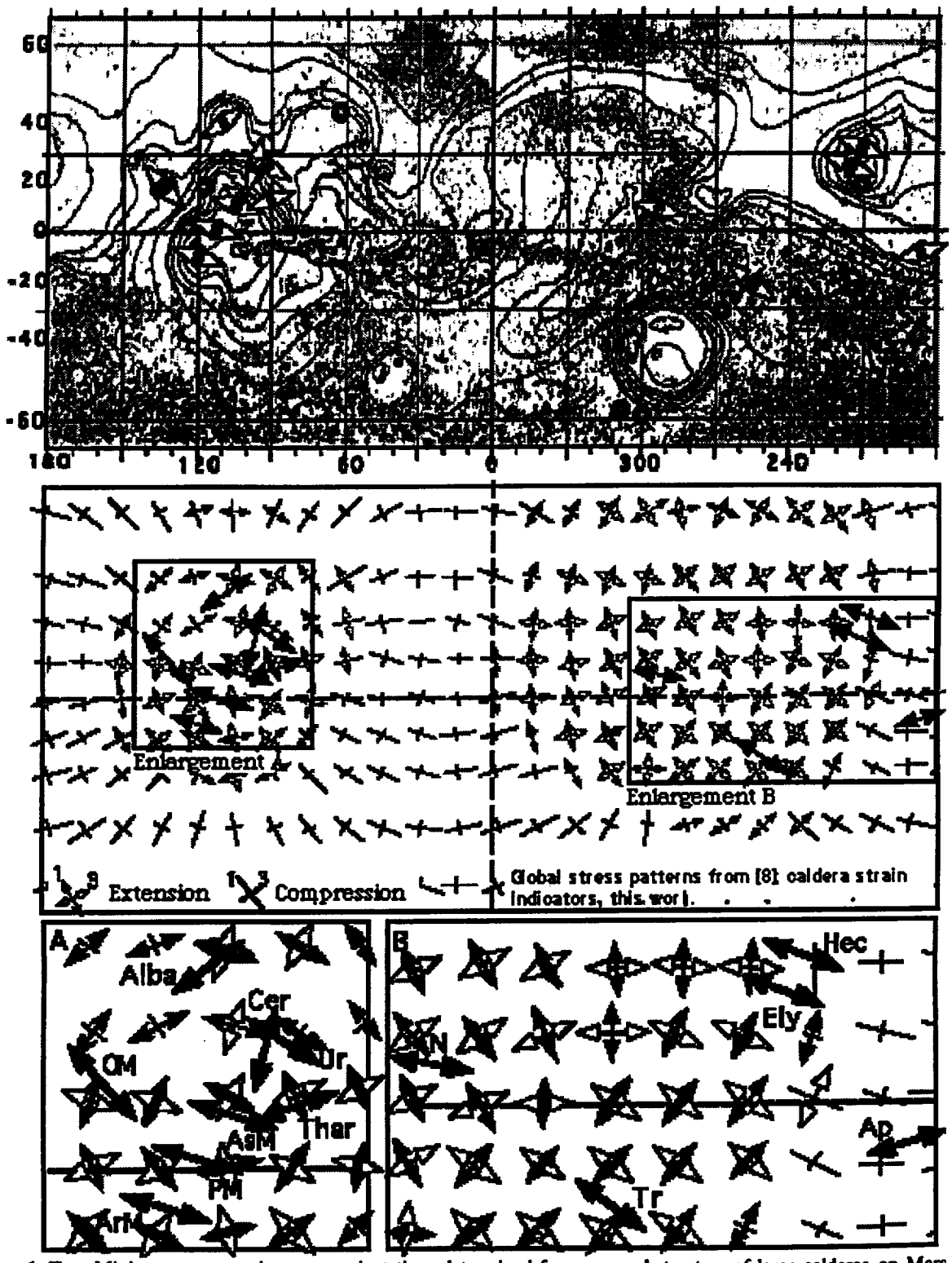

Figure 1. Top: Minimum compressive stress orientations determined from mapped structure of large calderas on Mars [1]. Center: Stress orientations superimposed on global stress field predicted from topography [8]; bottom: Enlargement of main volcanic regions. Observed orientations are consistent with remote stresses predicted from isostatic flexure in many cases, but some calderas appear to have been strongly influenced by stresses within the crust due to slope and azimuthal variations in crustal strength.

MAGMA RESERVOIR FAILURE: IMPLICATIONS FOR VOLCANO GROWTH ON VENUS AND MARS

Eric B. Grosfils[1] and James W. Head[2]; [1]Geology Department, Pomona College, Claremont, CA 91711, egrosfils@pomona.edu; [2]Department of Geological Sciences, Brown University, Providence, RI 02912.

Overview: Data obtained from a numerical model of magma reservoir failure, combined with observational constraints, provide insight into the conditions which promote volcano growth on Venus and Mars. On Venus, gradual deepening of an oblate ellipsoidal reservoir in a host rock subjected to uniaxial strain is consistent with the eruptive sequence preserved at Sapas Mons; further work is required to determine if this sequence is representative of other venusian edifices. On Mars, however, many eruptive sequences are known to be similar. These are most consistent with the presence of an oblate ellipsoidal reservoir located in a host which relaxes from uniaxial strain to lithostatic stress over time.

Introduction: Observational evidence, including calderas and laterally extensive dike swarms, indicates that magma reservoirs exist beneath and have fed many large volcanic edifices on Venus and Mars [1,2]. Understanding the mechanical evolution of the reservoirs can therefore provide insight into how these volcanoes develop and grow. The interplay between and relative importance of the factors which control reservoir failure, however, is not yet well understood. Excess pressure derived from repeated magma injection is uniform throughout the reservoir and thus, while this pressure may drive fracturing, other factors must dictate where the reservoir wall fails. Recent studies [3,4], building upon earlier efforts (*e.g.*, [5-7]), have identified a number of different factors which may control the point at which a reservoir fails; however, no published model explicitly incorporates them all, and conflicting conclusions are often drawn. Using a numerical model which incorporates all the parameters identified by earlier authors, we systematically re-evaluate how these factors contribute to reservoir failure [8]. Here we briefly summarize the results and, through comparison with observations from Venus and Mars, consider possible implications for edifice growth on each planet.

Model: Using an axisymmetric finite element method, we treat the reservoir as an internally pressurized ellipsoid within an elastic host. The left hand boundary of the mesh, which defines the rotation axis of the system, is free to slip in the vertical direction. The upper surface is pinned at the right end to anchor the mesh but is otherwise free, while depth-dependent vertical and horizontal forces, respectively, are applied to the bottom and right hand sides of the region to create a reference state of stress in the host rock. Forces applied normal to the reservoir walls reflect both excess pressure and a hydrostatic term. The program evaluates stresses for each element in polar cylindrical coordinates, then calculates the stresses normal and parallel to the reservoir walls to determine where tensile failure first occurs.

Summary of Results: The point at which failure first occurs, summarized in Table 1, is controlled primarily by the interaction between three parameters. These are: (a) the reference state of stress in the host rock; (b) the aspect ratio of the reservoir; and, (c) the size of the reservoir relative to its depth below the surface. Compared to these, the density difference between host rock and magma as a function of depth, even under extreme non-neutral buoyancy conditions, has only a minimal impact upon the failure location.

For a spherical magma body within a host rock subjected to either uniaxial strain or lithostatic stress, the most common point of failure is near the crest of the reservoir. This should promote vertical dike emplacement and centralized eruptions. Under lithostatic conditions, however, increasing the reservoir's proximity to the surface promotes rotation of the failure point away from the crest, producing stresses more consistent with either ring dike or cone sheet intrusion.

If a magma body approximates an oblate ellipsoid, the host rock stress state becomes more important. When the host is subjected to lithostatic stress, the reservoir always fails near its midpoint. (Note that sill injection is favored over lateral (radial) dike intrusion, contrary to results reported elsewhere [4].) But, when the host rock is subjected to uniaxial strain an oblate reservoir continues to fail near its crest. Mathematically, this location is only weakly favored relative to all other points on the reservoir wall. In practice, failure may therefore occur nearly anywhere in response to subtler effects than those we have treated. Irrespective of where failure takes place, however, dike injection is favored, and thus anything from vertical dikes feeding central eruptions to lateral dike intrusion can plausibly occur.

TABLE 1: Point of Failure in Degrees of Arc Relative to Top of Chamber and Possible Intrusion Style

HOST ROCK STRESS STATE & RESERVOIR DEPTH		RESERVOIR SHAPE: Spherical — Host Rock Density Model: Uniform	2-Layer	Gradual Δ (*)	DEPTH	Oblate — Density Model: Gradual Δ (*)
Uniaxial Strain	Shallow	0° vertical dike	0° vertical dike	0° vertical dike	Shallow	0 - 90° dike
	Deep	0° vertical dike	0° vertical dike	0° vertical dike	Deep	0° vertical dike
Lithostatic Stress	Shallow	45° ring dike; cone sheet	30° ring dike; cone sheet	45° ring dike; cone sheet	Shallow	90° lateral sill
	Deep	0° vertical dike	0° vertical dike	0° vertical dike	Deep	90° lateral sill

(*) Host density follows exponential form reflecting compaction of basaltic material (see *Head & Wilson* , 1992)

Discussion: On Mars, many of the volcanoes exhibit a common eruptive sequence [9]. Initial edifice construction occurs upon a thick accumulation of pre-edifice plains via persistent centralized eruption from a deep-seated magma reservoir. Eventually, however, the locus of eruption switches from a point near the summit to multiple flank locations. This sequence eliminates uniaxial strain and a spherical reservoir as well as lithostatic stress and an oblate reservoir, as neither combination facilitates the observed transition in eruption style. The sequence of events is consistent with, however, either variation in reservoir depth relative to the summit as the volcanoes grow or changes in the host rock state of stress as a function of time; in either instance the presence of an oblate reservoir is implied. (Note: The possible role played by edifice stresses is discussed elsewhere [10].) If reservoir depths change, they must grow shallower with time. It is unlikely, however, that reservoirs move to shallow enough depths for rotation from vertical to lateral failure to occur, as both observational evidence and theoretical calculations suggest that reservoirs on Mars form and remain at great depth [2,11]. It is perhaps more plausible, therefore, that a change in the host rock stress from a condition of uniaxial strain to a situation more closely approximating lithostatic is consistent with the observed sequence of eruptive events at volcanoes on Mars.

On Venus, fewer eruptive sequences have been rigorously evaluated. Here we consider the sequence documented at Sapas Mons [12], where early emplacement of lateral dikes and numerous flank eruptions were gradually superseded by centralized eruptions. Within the context of our modeling results, the observed variation in the eruptive sequence cannot be produced by either uniaxial strain and a spherical reservoir or by lithostatic stress and an oblate reservoir; furthermore, lateral diking is quite inconsistent with a spherical reservoir and lithostatic stress. The entire sequence can be explained by an oblate reservoir subjected to uniaxial strain, however, provided that the reservoir deepens relative to the summit of the volcano as the edifice grows. This interpretation suggests that uniaxial strain persistently defined the reference state of stress beneath Sapas Mons as it formed. Intriguingly, one way uniaxial strain could occur is if lava erupted at the surface gets buried beneath subsequent deposits, a situation broadly consistent with the process of plains emplacement on Venus. In addition, the oblate geometry inferred for the reservoir and its relative deepening as the edifice grows are both consistent with theoretical predictions [1]. To better constrain our model results and the reference state of stress beneath venusian edifices in general, however, we need to know whether the eruptive sequence at Sapas Mons is typical of other volcanoes, and we need to derive new ways to constrain the subsurface geometry of magma reservoirs using surface observations.

References: 1] Head & Wilson, *JGR, 97*, 3877, 1992; 2] Wilson & Head, *Rev. Geophys, 32*, 221, 1994; 3] Sartoris et al., *JGR, 95*, 5141, 1990; 4] Parfitt et al., *JVGR, 55*, 1, 1993; 5] Anderson, *Proc. R. Soc. Edinburgh, 56*, 128, 1936; 6] Blake, *Nature, 289*, 783, 1981; 7] McTigue, *JGR, 92*, 12931, 1987; 8] Grosfils, *Ph.D. Thesis*, Brown Univ., 1996; 9] Crumpler & Aubele, *Icarus, 34*, 496, 1978; 10] McGovern & Solomon, *JGR, 98*, 23553, 1993; 11] Zuber & Mouginis-Mark, *JGR, 97*, 18295, 1992; 12] Keddie & Head, *EM&P, 65*, 129, 1994.

LUNAR MARE BASALT VOLCANISM: EARLY STAGES OF SECONDARY CRUSTAL FORMATION AND IMPLICATIONS FOR PETROGENETIC EVOLUTION AND MAGMA EMPLACEMENT PROCESSES.

J. W. Head, Department of Geological Sciences, Brown University, Providence RI 02912; L. Wilson, Planetary Science Group, Environmental Sciences Division, Institute of Environmental and Biological Sciences, Lancaster University, Lancaster LA1 4YQ, UK and D. Wilhelms, 2027 Hyde St. #6, San Francisco CA 94109. (James_Head_III@Brown.edu)

Introduction: Lunar mare basalt deposits are an example of a vertically accreting secondary crust (derived from partial melting of planetary mantles) superposed on a platform of primary crust (derived from accretional and related heating) [1]. The small total area covered by mare deposits (~17% of the surface) [2] and the small volume (~1 x 10^7 km^3) [2] are such that the stratigraphy, fluxes and modes of emplacement can be documented and studied, particularly with the availability of Clementine multispectral imaging [3] and the complementary Apollo and Luna sample collections [e.g., 4-6]. These data can then be used to test models for the origin, ascent and eruption of basaltic magmas, and to document the early stages of secondary crustal formation and evolution. Here we review the emerging new stratigraphy, estimates of flux, the characteristics of surface deposits and implications for modes of emplacement, and emerging constraints on petrogenetic models for generation and emplacement of secondary crustal magmas.

Stratigraphy, Duration and Flux: In general, photogeologic, remote sensing and returned sample studies [7,8] show that mare volcanism began prior to the end of heavy bombardment (period of cryptomare formation [9]), in Early Imbrian and pre-Nectarian times, and continued until the Copernican Period, a total duration approaching 3 billion years. Recent analyses have shown that there were widespread mare regions during the cryptomare period comparable in area to presently exposed maria such as Serenitatis [15-17]. For later deposits, detailed analyses is revealing the range of volumes typical of individual eruptions [13] and Clementine data are revealing the compositional affinities and volumes of units in individual basins and regions [14-16]. The source of heat required for melting and depth of origin is a major outstanding question in the petrogenesis of mare basalts [6, 18] and the onset of mare-type volcanism is a key to the understanding of some types of models [19] for the origin of mare basalt source regions. Increasing detection of cryptomaria has clearly demonstrated that mare volcanism began and was areally extensive [15-17, 20] prior to the formation of Orientale, the last of the large impact basins, at about 3.8 Ga [7]. Presently unresolved is the actual age of onset and areal and volumetric significance of this early mare-type volcanism. New information on the diversity and distribution of mare basalts as a function of time are beginning to accumulate from the analysis of Clementine data. Initial Apollo models emphasized the high-Ti nature of A11 basalts and the low-Ti nature of A12 basalts leading to the hypothesis that melting of the mare basalt source region began at the ilmenite-rich residuum and deepened with time into the mantle [18]. Remote sensing data from unsampled western maria [21] showed, however, that young high-Ti basalts were widespread and that they were largely of Eratosthenian age [4]. These and subsequent analyses [e.g., 15, 22] have shown that each of the mare basins are characterized by a diversity of mare basalt volcanic fill. Utilizing these data and our own analyses, we have produced a stratigraphic synthesis of mare basalts in individual basins and regions; this synthesis shows that temporal compositional heterogeneity is at least as important as sequential heterogeneity and provides information on the flux. Abundant geologic evidence shows that the vast majority of observed volcanic deposits (>90%, ~9.3 x 10^6 km^3) were emplaced in the Late Imbrian Period, spanning 600 Ma from about 3.8 to 3.2 Ga [7, 9, 23]; new crater-count data continue to confirm this and to place diverse stratigraphically dated mare deposits in this period [e.g., 17]. A wide range of basaltic compositions was being emplaced in virtually all the nearside mare basins, with earliest and intermediate deposits dominated by (but not confined to; e.g., see [15]) high-Ti basalts; later deposits of this period are dominantly low-Ti and represent the major late fill of nearside basins (e.g., Crisium, Serenitatis, Imbrium, Procellarum). The emerging picture is that the maximum period of production, ascent, and emplacement of mare basalts was between 3.8 and 3.2 Ga; magmas produced during this period were diverse in space and time, but dominated by an early phase of high-Ti basalts. Following this, <5% of the total volume of mare basalts was emplaced during the Eratosthenian Period (spanning ~2.1 Ga); a few of the latest flows may extend into the Copernican Period. Predominantly high-Ti basalts were emplaced largely on the central and western nearside (Imbrium and Procellarum). The low overall volume and low average effusion rate of the latest deposits is partly due to global cooling and the increasingly compressional state of stress in the lithosphere [18], both factors minimizing production of basaltic magmas and their ascent to the surface. A key conclusion is that the heat source for melting of parental material was operating for possibly as long as an additional 2 Ga, and that it was producing high-Ti basalts extruded over a limited portion of the lunar surface. In summary, mare deposits are testimony to the production and extrusion of mare basalts for a period of at least 2 Ga and perhaps as long as 3 Ga; surface volcanism, however, has not been volumetrically significant on the Moon since about the late Archean on Earth. Mare volcanic flux was not constant, but peaked during the Late Imbrian Period; average global volcanic output rate during this peak period was ~10^{-2} km^3/a, comparable to the present local output rates for individual volcanoes on Earth such as Kilauea, Hawai'i. Some

single eruptions associated with sinuous rilles may have lasted about a year and emplaced 10^3 km^3 of lava. The flux was variable in space and time during this period, and the patterns revealed by the stratigraphy show evidence for regional concentrations of sources and compositional affinities; these patterns are the basic data for defining the configuration, size, and density of mantle source regions throughout the period of mare basalt emplacement. Evidence for emplacement style suggesting that magmas are commonly delivered to the surface in large quantity through dikes originating from depth include areally extensive lava flows [25], sinuous rilles attributable to thermal erosion [26], lack of large shield volcanoes [27], and evidence for the emplacement of large dikes in the vicinity of the surface [28]. The low density of the lunar highlands crust provides a density barrier to the buoyant ascent of mantle melts [29] and ascending diapirs are likely to stall at a neutral buoyancy zone there, before reservoir overpressurization propagates dikes toward the surface [9]. In summary, these data provide an emerging picture of the nature, flux, and mode of emplacement of lunar mare deposits.

Testing Models of Petrogenesis and Modes of Emplacement: These data on mare heterogeneity in time and space can be used to test models for the petrogenesis and mode of emplacement of mare basalts. As an example, in one model [19], the dense ilmenite-rich (with high concentrations of incompatible radioactive elements) and underlying Fe-rich cumulates forming at the base of a stratified lunar differentiate are negatively buoyant and sink to the center of the Moon. Subsequent radioactive heating causes mantle melting and diapiric rise of magmas. The low-density highland crust acts as a density barrier to the buoyant ascent of mare basalt magmas, likely causing them to stall and overpressurize, sending magma-filled dikes to the lunar surface. This density-barrier factor may be responsible for much of the areal difference in distribution of mare basalt deposits, most notably in the nearside-farside asymmetry [9]. We compare the predictions of this model to the stratigraphic record of mare basalt magmas and find qualitative agreement with this petrogenetic model. The emerging details of the stratigraphic record, and increasing ability to read throughout the primary crustal density filter permits us to begin to constrain aspects of this model and examine others.

References: 1] S. Taylor (1989) *Tectonophysics, 161*, 147; 2] J. Head (1975) *Origins of Mare Basalts*, LPI, 66; 3] A. McEwen et al. (1994) *Science, 266*, 1858; 4] L. Nyquist and C. Shih (1992) *G&CA, 56*, 2213; 5] C. Neal and L. Taylor (1992) *G&CA, 56*, 2177; C. Shearer and J. Papike (1994) *G&CA, 57*, 4785; 6] J. Delano (1986) *JGR, 91*, D201; 7] D. Wilhelms (1987) *USGS PP-1348*, 302 pp; 8] J. Head, *RGSP, 14*, 265, 1976; *BVSP*, Pergamon, 1981; 9] J. Head and L. Wilson (1992) *G&CA, 56*, 2155; 10] J. Head et al. (1993) *JGR, 98*, 17149; 11] R. Greeley et al. (1993) *JGR, 98*, 17183; 12] B. Hawke *et al.* (1993) *GRL, 20*, 419; I. Antonenko et al. (1995) *EMP, 69*, 141; J. Mustard and J. Head (1996) *JGR, 101*, 18913; 13] A. Yingst and J. Head (1996) *LPSC 27*, 1477; *ibid.*, 1479; 14] A. Yingst and J. Head, this volume; 15] M. Staid et al. (1996) *JGR, 101*, 23213; 16] H. Hiesinger et al. (1996) *LPSC 27*, 545; *ibid.*, 547; 17] H Hiesinger et al., this volume; 18] S. R. Taylor (1982) *Planetary Science: A Lunar Perspective*, LPI; 19] P. Hess and E. Parmentier (1995) *EPSL, 134*, 501; 20] J. Bell and B. Hawke (1984) *JGR, 89*, 6899; B. Hawke et al. (1991) *GRL, 18*, 2141; 21] C. Pieters (1978) *PLPSC 9*, 2825; 22] J. Johnson et al. (1991) *JGR, 96*, 18861; 23] W. Hartmann et al. (1981) *BVTP*, 1049; 24] S. Solomon and J. Head (1980) *RGSP, 18*, 107; 25] G. Schaber (1973) *PLSC 4*, 73; 26] G. Hulme (1973) *MG, 4*, 107; M. Carr (1973) *Icarus, 22*, 1; 27] J. Head and L. Wilson (1991) *GRL, 18*, 2121; 28] J. Head and L. Wilson (1993) *PSS, 41*, 719; 29] S. Solomon (1975) *PLPSC 6*, 1021.

COMPOSITION AND TEXTURES OF IMPACT AND VOLCANIC GLASSES IN THE 79001/2 CORE. C. M. Weitz, M. J. Rutherford, and J. W. Head III, Department of Geological Sciences, Brown University, Box 1846, Providence, RI 02912.

Introduction: We have studied thin sections from the 79001/2 core taken on the rim of the 90 m diameter impact crater Van Serg. The core is a mixture of basalt and highland fragments, lithics, agglutinates, and impact and volcanic glasses. The core is significantly different from the 74001/2 core taken on the rim of the impact crater Shorty. While the 74001/2 core is composed of only orange glasses and their crystallized equivalents [1, 2] and therefore represents a stratigraphic section at depth, the 79001/2 core represents a mixture of components making up the regolith. Our interest in the 79001/2 core was to search for volcanic glasses and determine their relationship to those found at Shorty. Each of the 19 thin sections in the Van Serg core was studied and glasses were identified. Impact and volcanic glasses that had a unique texture were compositionally analyzed, as were 128 glasses from two thin sections in the core.

Approach: The thin sections were initially studied at the Johnson Space Center. Several distinct glasses were selected for probing using a Cameca SX-100 probe to produce digital elemental maps of Si, Al, Ti, Fe, and Mg. The thin sections were then transferred to Brown University where a Cameca Camebax was used to obtain quantitative measurements of glass compositions. For standards, we used a terrestrial basaltic glass composition. In addition, several beads from the Apollo 15 green glass (low-Ti) and the Apollo 17 74220 orange glass (high-Ti) were analyzed and re-normalized to values obtained by [3] for the Ap15 and Ap17 glasses. The re-normalized standards were then applied to the 79001/2 glass analyses. Spot size for each probe analysis was approximately 10 μm.

Figure 1

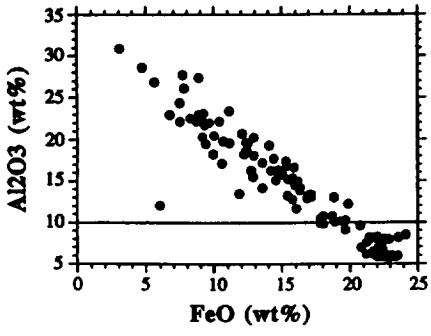

To distinguish between impact and volcanic glasses, we designated all glasses with <10 wt% Al_2O_3 and >10 wt% MgO compositions as volcanic because all the 25 lunar volcanic glasses identified by [3] fell within this category. Figure 1 shows a plot of FeO vs Al_2O_3 for the 128 glasses analyzed from two 79001/2 thin sections. The volcanic glasses below 10 wt% Al_2O_3 have the highest FeO content, supporting a more primitive and mafic composition.

Results for the Impact Glasses: The elemental maps were useful for identifying textures in the glasses and determining relative compositions. One particularly interesting and unique bead is 600 μm in diameter and is composed of an inner and outer zone, giving the appearance of an egg (figure 2). The outer zone is heterogeneous in composition and has a swirly orange/white texture in transmitted light. Its average composition is 10 wt% MgO, 11 wt% Al_2O_3, 44 wt% SiO_2, 10 wt% CaO, 6 wt% TiO_2, and 18 wt % FeO. Interspersed in the outer zone are small metal blebs with compositions of 89-94 wt% Fe, 6-10 wt% Ni, and 0.8 wt %Co. The inner zone ("the yolk") has a homogeneous composition of 36 wt% MgO, 37 wt% SiO_2, and 26 wt% FeO and is clear in transmitted light. The inner zone is an olivine crystal that was originally part of a basalt or an ultramafic rock. During an impact event, the olivine fragment became incorporated into an impact glass and partially melted at the contact zone. As the bead later cooled, smaller olivine crystals grew into the adjacent impact glass.

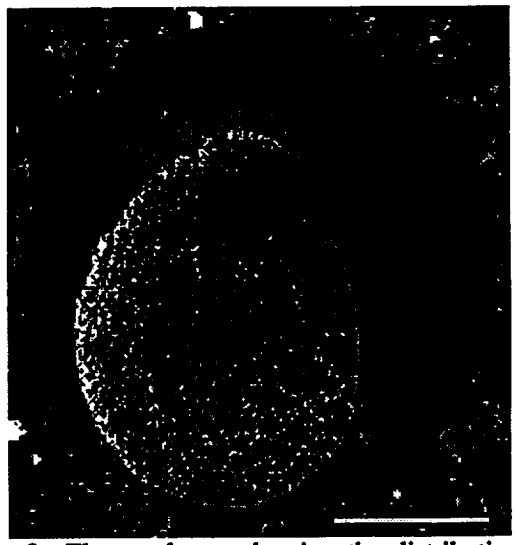

Fig. 2. Elemental map showing the distribution of MgO in an impact bead. Bar at bottom is 200 μm. Black dots in outer zone are Fe-rich metal blebs.

Many of the impact glasses have small metal blebs interspersed throughout them. Unlike the Fe-Ni metal blebs identified in the 74001/2 core which formed by oxidation of graphite in a magma at depth [4], the

metal blebs in the impact glasses formed by reduction at the surface [5]. One 200 μm yellow glass bead has large metal blebs at the rim that progressively decrease in size moving inward. The correlation between bleb size and location from the rim suggests that the bead was molten and spinning in the air after formation, causing the metals to redistribute by size. Many other impact glasses have metal blebs only at their rims but all the blebs appear the same size. Other blebs inside impact glasses are located only between cracks in the glasses. Thus, the location and occurrence of metal blebs in the impact glasses appears to be a function of several factors. Finally, the larger impact glasses show partial crystallization and several clear glasses have brown devitrification textures, similar to those identified in the Apollo 17 orange glasses [6].

Results for the Volcanic Glasses: Of the 128 glasses analyzed, 51 had <10 wt% Al_2O_3 and >10 wt% MgO and were considered volcanic. The glasses are plotted as a function of MgO, TiO_2, and FeO in figures 3 and 4. The majority of volcanic glasses analyzed in this study fall within one of the five types identified by [7] or their fractionation trends for the Apollo 17 glasses. However, several do not and may represent volcanic glasses transported by impacts from other locations or from smaller pyroclastic eruptions in the region.

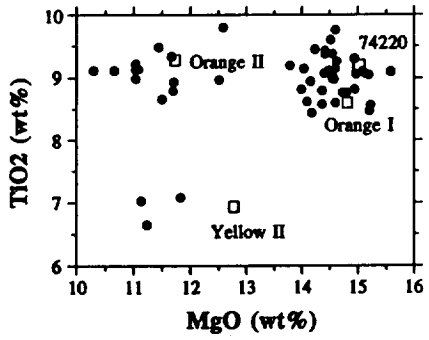

Fig. 3. MgO vs TiO_2 for the volcanic glasses analyzed. Squares represent the most primitive (i.e. highest MgO) for the different glass types (74220, Orange I, Orange II, and Yellow II) identified by [7]. (VLT glasses not shown).

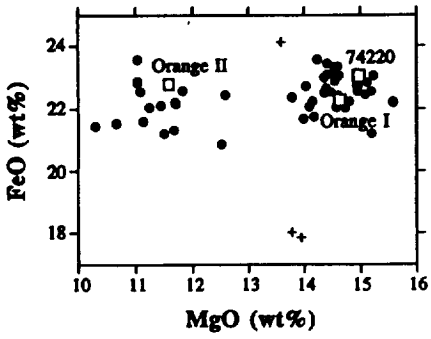

Fig. 4. MgO vs FeO for the volcanic glasses. The crosses represent the three very low-Ti (0.5-2.1 wt%) glasses identified in this study.

Discussion: The dark mantle deposit of Taurus-Littrow is dominated by the 74220 glasses and their crystallized equivalents (black beads). Compositional analyses of the Shorty Crater core [8] indicate that the orange glasses are compositionally the same throughout the entire core and no fractionation trend can be identified within the 74220-type. However, the other glass types, including the Orange I, Orange II, and Yelow II all show limited fractionation trends [7]. This raises the important issue as to why the 74220 glasses experienced little, if any fractionation, while the other glasses did. The answer may lie in the style of eruption that emplaced the glasses.

Compared to the 74220 glasses, the other types most likely erupted from smaller eruptions in the area and did not contribute a substantial amount of material to the dark mantle deposit. The dark mantle deposit itself, which covers 1000's of km^2 in area and is probably several meters thick, is thought to have been erupted from a source vent located to the northwest which was later buried by the younger mare of Serenitatis [6]. To expel beads for 100's of kms to form a continuous deposit requires high mass effusion rates. For this larger, high mass effusion eruption, the ascending magma may not have had sufficient time to cool and fractionate. In contrast, the smaller eruptions that emplaced the other glasses may have stalled at depth until a foam layer composed of volatiles had built up sufficient pressure to cause an eruption. During the time that the magma remained stalled below the surface, it could have begun to cool and fractionate to produce the observed fractionation trends in the data. In addition, the higher MgO contents for the 74220-type support a more primary composition. A likely vent for the other types of glasses is the source head of the sinuous rille Rima Carmen located in the southern portion of the Taurus-Littrow deposit. Theoretical calculations [9] indicate that if only a few wt% of clasts ejected during the eruption are the submillimeter beads then they can be ejected as far away as the Van Serg location (~ 40 km distance).

References: [1] Heiken, G. H., D. S. McKay, and R. W. Brown, *Geochim. Cosmochim. Acta., 38*, 1703-1718, 1974; [2] Heiken, G. H., and D. S. McKay, *Proc. LPSC IX*, 1933-1943, 1978; [3] Delano, J. W., *Proc. LPSC XVI*, 201-213, 1986; [4] Weitz, C. M., M. J. Rutherford, and J. W. Head, *Geochim. Cosmochim. Acta., in press*, 1997; [5] Baedecker, P. A., C. L. Chou, and J. T. Wasson, *Proc. LPSC 3rd*, 1343-1359, 1972; [6] Weitz, C. M., J. W. Head, and D. S. McKay, *LPSC XXVII*, 1411-1412, 1996; [7] Delano, J. W., and D. H. Lindsley, *Proc. LPSC 14th*, B3-B16, 1983; [8] Blanchard, D. P., and J. R. Budahn, *Proc. LPSC IX*, 1969-1980, 1978; [9] Wilson, L., and J. W. Head, *J. Geophys. Res., 86*, 2971-3001, 1981.

GEOLOGY OF THE LUNAR REGIONAL DARK MANTLE DEPOSITS AS SEEN BY CLEMENTINE UVVIS DATA. C. M. Weitz, J. W. Head III, and C. M. Pieters, Department of Geological Sciences, Brown University, Box 1846, Providence, RI 02912 (Catherine_Weitz@Brown.edu).

Introduction: We have used calibrated Clementine UVVIS data to map the geology and analyze spectra from several regional Dark Mantle Deposits (DMD) on the Moon, including Taurus-Littrow (TL), Rima Bode (RB), Sulpicius Gallus (SG), Aristarchus Plateau (AP), and Orientale (OR). Regional DMD formed from pyroclastic eruptions and are composed of either volcanic glasses or crystallized beads. Unlike smaller localized dark mantle deposits, like those in Alphonsus and Franklin craters, which are only a few kms in diameter and are produced from vulcanian eruptions [1, 2], regional DMD cover tens of km and indicate higher volume fluxes and plume heights. The crystallinity of the volcanic beads in a DMD is a very useful parameter for determining the cooling rates within the volcanic plume, with glasses indicating high cooling rates in a low optical density plume. Telescopic spectral data of the deposits [3, 4, 5] indicate that TL and RB are dominated by crystallized black beads, SG is an equal mixture of glasses and black beads, while AP is dominated by the glasses. More recent Clementine data of the OR deposit on the lunar farside has shown that it is composed of volcanic glasses similar to those in the AP deposit [6].

Taurus-Littrow Deposit: The TL deposit is the only RDMD where samples were collected. The Apollo 17 mission retrieved several soil samples of the dark mantle and has shown that it is a mixture of high-Ti orange glasses and their crystallized equivalents (black beads), with the crystallized beads dominating the deposit [7, 8]. A drill core taken on the rim of the 120 m diameter impact crater Shorty showed that the orange glasses erupted earlier and then progressively changed to an eruption producing the black beads [9].

High-resolution Clementine UVVIS images (106 m/pixel) of the Taurus-Littrow Valley, including the Apollo 17 site, have been used to correlate the Clementine data to ground truth observations and high resolution Apollo photographs. In general, our interpretations using the Clementine data agree well with the geologic map by Wolfe et al. [10] produced using Apollo photographs. The DMD is darkest just north of the light mantle deposit and in the southeast of the valley away from the crater clusters. In contrast, the central portion of the valley floor is dominated by the spectra of the crater clusters and their ejecta. Adjacent to the highlands (South and North Massifs), the spectra is dominated by mature highland soils that have mass wasted onto the valley floor and mixed with the local soils. Ejecta from Shorty Crater is visible in the Clementine data because of its low albedo due to the dark mantle it exposed underneath the light mantle deposit.

The Clementine data also show a mafic signature in the walls of the craters Camelot, Sherlock, Steno-Apollo, Powell, Faust, and Emory. These craters, all of which are between 0.5-1 km in diameter and most of which are considered to be secondaries from Tycho [10], have exposed the underlying basalts in the valley. The crater Steno-Apollo has the highest 0.75/0.95 μm signature of all the crater clusters in the valley, suggesting that it is the youngest. A 0.1 km diameter crater and its smaller neighbor in the southern edge of the Sculptured Hills were mapped among the youngest craters in the valley [10]. In the Clementine data, the two craters appear as one larger crater with a very strong noritic signature. The northeastern edge of Bear Mountain also has a noritic signature, perhaps associated with a young crater, while the rest of the Mountain is composed of anorthositic breccia.

The Clementine UVVIS data (180 m/pixel) for the TL DMD to the northwest of the Taurus-Littrow valley show a low reflectance, high UV/VIS ratio, and a relatively featureless spectra from 0.4 to 1.0 μm, characteristic of the black beads. Fresh craters in the surrounding low-Ti mare of Serenitatis have a basaltic spectra while the larger fresh craters in the DMD appear more noritic in composition. The surrounding highlands have either a spectra for anorthosite, norite, or a mixture of the two. Therefore, it appears that many of the larger craters in the DMD are penetrating to underlying noritic highlands. In contrast, the craters in the Taurus-Littrow valley exposed underlying mare. Young small craters in the highlands and DMD have exposed fresher dark mantle beneath the regolith while small craters in the north have penetrated through a large 7.2 km diameter crater's bright ejecta blanket, exposing the underlying DMD.

Rima Bode Deposit: The Rima Bode DMD has a spectra similar in shape to the TL DMD but slightly higher in reflectance; hence, the DMD is dominated by the crystallized black beads and may have been mixed with more highlands than at TL. Overall, the deposit is also very similar in shape and size to the TL DMD, suggesting that the two DMD had a similar eruptive history. The DMD has been partially covered by mare to the west and south, although small kapukas of the DMD are still visible in the south. The spectra for the perched lava pond mapped by [4] has a similar spectra to the low-Ti mare soils of Serenitatis. Moving radially outward, the DMD is higher in reflectance and more patchy, supporting that it is thinner and has mixed with the surrounding highlands [3]. The spectra for the highlands indicate a mixture of anorthositic breccia and norite.

Sulpicius Gallus Deposit: Photographs of the deposit taken during the Apollo 17 mission showed layers of orange and red glasses exposed in several crater walls [11]. Spectra from the Clementine UVVIS data show that the deposit has the highest reflectance of all the RDMD analyzed in this study and a glass band is readily visible. The high reflectance may be due to the extensive mixing of the deposit with the surrounding highlands of southwestern Mare Serenitatis. Unfortunately, we are unable to distinguish between the red and orange glass layers in the DMD at this low spatial (155 m/pixel) and spectral resolution. Luchitta and Schmitt [11] also identified dark material on the inside of a 1.5 km diameter fresh impact crater located in the mare and suggested that a dark mantle layer occurred beneath the younger mare at the edge of the Serenitatis basin. However, the Clementine data show a bright interior for this crater with a strong low-Ca pyroxene absorption, indicating that the dark interior is in fact young, fresh basalt. The Apollo 17 photos also showed a 5.5 km-long kidney-shaped depression with orange and red layers visible in its walls [11]. Clementine data for the depression show a low 0.4/0.75 μm and high 0.75/0.95 μm ratio around the walls, supporting a mafic composition in the walls but no dark mantle could be resolved.

Mare ponds in the highlands are visible to the south and in the western portion of the DMD. Numerous small craters with a higher reflectance, steeper UV/VIS, and stronger glass band compared to the surrounding DMD appear to have excavated fresher dark mantle. The large 12 km diameter crater, Sulpicius Gallus, in the mare has a spectra of both norite and basalt in its walls, indicating that the crater penetrated to the depth of the contact between the mare and highlands.

Aristarchus Plateau Deposit: Telescopic observations showed that the Plateau was covered by orange/red volcanic glasses [4, 12]. Preliminary Clementine observations of crater ejecta in the DMD were used to estimate a thickness of 10-30 m for the deposit [13]. The DMD is darkest to the northwest, most likely due to the mixing and burial of the dark mantle by the Aristarchus crater located to the southeast. Numerous small bright hills interspersed throughout the DMD are composed of anorthositic material and presumably represent ejecta from either Aristarchus crater or from the formation of Imbrium basin. The walls of Vallis Schroteri and the smaller rilles have a mafic signature supporting that mare exists beneath the DMD [13]. There are several small patches of dark mantle with lower 0.4/0.75 μm ratios nestled in the DMD. These patches may reflect variations in glass type, maturity, and/or mixing.

Orientale Ring Deposit: The ring deposit is centered on the Montes Rook in the southwestern portion of the Orientale basin. Previous observations of the OR deposit by the Galileo spacecraft showed that it was composed of a mixture of pyroclastics and highland materials [14, 15] but the crystallinity of the beads could not be determined. The Clementine UVVIS data now show that the DMD is composed of volcanic glasses similar to those at AP, indicating high cooling rates in a low optical density plume. The deposit is 154 km across and has an 18-km long elongate depression at its center which we interpret as the source vent of the DMD. The deposit is darkest and widest in the north but thinner and brighter elsewhere due to mixing with the highlands.

The vent has a noritic signature similar to that found in the local crater walls and no lavas can be seen surrounding the vent, indicating that the vent is a collapse feature and no mare erupted in association with the emplacement of the glasses. Based upon the distribution of the deposit and using the elongate central depression as the source vent, the deposit can best be modeled by an eruption from a foam layer at the top of a dike that stalled a few kms below the surface. The volcanic plume was umbrella-shaped, similar to those seen on Io, with eruption velocities from 350-400 m/s and a plume height of 40 km [6].

Conclusions: The Clementine UVVIS data with its 5-channel spectral resolution and relatively high spatial resolution has enabled us to provide new information about the regional DMD and the geology of the surrounding region. In particular, the identification and modeling of the OR deposit, which is the first annular regional DMD identified on the Moon, has provided insight into another style of lunar pyroclastic eruption. Continued analysis of the other orbits that cover these deposits as well as a study of the remaining regional DMD will help us to understand how they formed and further our knowledge about the explosive volcanic history of the Moon.

REFERENCES: [1] Head, J. W., and L. Wilson, *Proc. LPSC 10*, 2861-2897, 1979; [2] Hawke, B. R., C. R. Coombs, L. R. Gaddis, P. G. Lucey, and P. D. Owensby, *Proc. LPSC 19*, 255-268, 1989; [3] Pieters, C. M., T. B. McCord, S. H. Zisk, and J. B. Adams, *J. Geophys. Res., 78*, 5867-5875, 1973; [4] Gaddis, L. R., C. M. Pieters, and B. R. Hawke, *Icarus, 61*, 461-489, 1985; [5] Hawke, B. R., C. R. Coombs, B. A. Campbell, P. G. Lucey, C. A. Peterson, and S. H. Zisk, *Proc. LPSC 21*, 377-389, 1991; [6] Weitz, C. M., J. W. Head III, and L. Wilson, *AGU Fall Abstracts*, F449, 1996; [7] Heiken, G. H., D. S. McKay, and R. W. Brown, *Geochem et Acta, 38*, 1703-18, 1974; [8] Heiken, G. H., and D. S. McKay, *Proc. LPSC 9*, 1933-1943, 1978; [9] Heiken, G. H., and D. S. McKay, *PLPSC 8*, 1977; [10] Wolfe, E. W. et al., USGS Prof. Paper 1080, 1981; [11] Lucchitta, B. K. and H. H. Schmitt, *Proc. LPSC 5*, 223-234, 1974; [12] Zisk et al., *The Moon, 17*, 59-99, 1977; [13] McEwen, A. S., M. S. Robinson, E. M. Eliason, P. G. Lucey, T. C. Duxbury, and P. D. Spudis, *Science, 266*, 1858-1862, 1994; [14] Pieters, C. M., et al., *J. Geophys. Res., 98*, 17127-17148, 1993; [15] Greeley, R. et al., *J. Geophys. Res., 98*, 17183-17206, 1993.

Factors Controlling the Depths and Sizes of Magma Reservoirs in Martian Volcanoes. L. Wilson[1,2] and J.W. Head[2]. [1]Environmental Science Division, Institute of Environmental and Biological Sciences, Lancaster University, Lancaster LA1 4YQ, U.K. L.Wilson@Lancaster.ac.uk [2]Department of Geological Sciences, Brown University, Providence RI 02912, U.S.A. James_Head@Brown.edu

We investigate how the variation of density with depth controls the locations of magma reservoirs in basaltic volcanoes on Mars, finding that reservoir centers should typically lie at depths of 9 to 13 km, and discuss stress controls on the vertical extents of reservoirs.

Magma reservoirs in basaltic volcanoes on Earth commonly develop with their centers at depths at which magmas are neutrally buoyant in the surrounding crust [1]. This implies that hydrostatic stresses dominate dynamic stresses in determining where in the crust the dikes and sills which ultimately develop into reservoirs come to rest, and there are theoretical reasons related to the ease with which dike tips propagate why this is likely to be the case [2]. A simple model [3] of the variation of crustal density ρ with depth h in basaltic volcanic areas assumes that the volcanic pile grows by deposition of fragmental or vesicular eruption products which then compact under gravity so that the void space V decreases exponentially with pressure P: $V = V_0 \exp(-\lambda P)$ where V_0 is the surface void space fraction and λ is a constant. If ρ_∞ is the limiting density of the crustal rocks at infinite compression, the definition of void space implies that the surface density $\rho_{surf} = \rho_\infty (1-V_0)$, and in general $\rho = \rho_\infty(1-V)$. Suitable integration of the definition of the pressure variation, $dP/dh = \rho g$, leads to

$$\rho(h) = \rho_\infty/[1 + \{V_0/(1-V_0)\} \exp(-\lambda\rho_\infty gh)]$$

$$P(h) = (1/\lambda) \ln[V_0 + (1-V_0) \exp(\lambda\rho_\infty gh)]$$

and the best fit [3] of these functions to density profiles in Hawai'i and Iceland on Earth, for which ρ_{surf} ~2200 kg m^{-3} (so that $V_0 = 0{\cdot}24$) and ρ_∞ ~2900 kg m^{-3}, gives $\lambda = 11{\cdot}8$ GPa^{-1}. We expect that λ will have a similar value on Mars, since the potential for density-altering processes other than simple compaction (e.g. hydrothermal fluids and secondary mineral deposition) existed for the martian volcanoes.

Table 1 shows the subaerial crustal density variations implied by this function using the observed $V_0 = 0{\cdot}24$ for Earth. A rising basaltic magma with a typical density of 2600 kg m^{-3} will be neutrally buoyant at a depth of 3 km, and it is at just this depth that the magma reservoir in the hawaiian volcano Kilauea is centred [4]. The corresponding density profile given for Mars (where the lower atmospheric pressure may lead to relatively vesicular eruption products [5]) uses a value of 0.325 for v_0. Also shown are the bulk densities as a function of depth for two candidate martian magmas which have liquid densities of 2600 kg m^{-3} (making them buoyant in the 2900 kg m^{-3} density crust at depth) and dissolved CO_2 contents in their source zone of 0.1 and 0.3 wt%. The symbols P, N and - indicate whether the magma is positively, negatively or neutrally buoyant in the crust. Progressive exsolution of the volatile with decreasing pressure (exacerbated by assuming that the volatile is the relatively insoluble CO_2) reduces the bulk magma density and, at the higher volatile content, causes the magma to reach a neutral buoyancy level (NBL) shallower than the 11.16 km depth appropriate to gas-free magma. Unless the magma is very CO_2-rich, however, magma reservoir growth is likely to be centred close to the 11 km NBL for this surface void fraction. Reducing V_0 decreases the NBL, to ~8 km for $V_0 = 0.25$; similarly increasing V_0 to 0.5 increases the NBL to ~16 km. These values should represent extremes of the range for Mars, suggesting that most magma reservoirs should be centred at depths between perhaps 9 and 13 km.

Magma reservoirs grow incrementally as a result of injections of fresh magma from below which increase the internal fluid pressure to the point where new dikes propagate from the

boundary. As a new dike cools it becomes part of the country rocks, but the thermal gradient near the boundary of the reservoir ensures that no dike cools to the point where no trace of its existence remains. The remains of previous dikes represent the best sites for subsequent dike growth because their tips, although becoming ever more rounded as cooling progresses, are locations of stress concentration at the reservoir margin. Driving pressures (country rock stress minus magma pressure) of only a few MPa are needed to re-activate meter-scale dike stubs [6], and repeated growth of dikes at a single point on the reservoir wall in this way leads to lateral rift zone formation. If old dike stubs cool beyond the point where they represent favored locations for wall rock failure, the reservoir walls must fail in tension or compression, requiring much larger stress differences across the boundary and making the site of failure (controlled by the stresses due to edifice topography) less predictable. This implies that martian sheild volcanoes without well-defined rift zones are those which are most likely to have had long repose periods between episodes of recharge and growth.

Geometric factors, plus the fact that the magma inside a reservoir tends to be slightly less compressible than the country rocks of the growing volcanic pile, means [7] that a smaller stress difference is needed to cause failure around the middle of a reservoir than at its roof or floor. In the lowest-stress-difference case of dike stub reactivation, the absolute pressure inside a martian reservoir centred at a depth of 11 km must be close to the country rock stress level, ~97 MPa. The equivalent for a reservoir on Earth centred at 3 km depth is 72 MPa. These pressures consist of the weight of the magma within the upper half of the reservoir plus an excess pressure in the magmatic fluid. On Earth, where hawaiian reservoirs have half heights of ~2 km, the magma weight is ~52 MPa implying an excess pressure of ~20 MPa. This excess pressure must be inherited from the processes of melt formation by pressure-release partial melting in the mantle. If similar processes, and hence excess pressures, occur on Mars, this implies magma weights of ~77MPa. This in turn implies that reservoir half-heights could be as large as 7 to 8 km, placing reservoir roofs as shallow as 3 to 4 km.

These geometric considerations have implications for the pressure gradients driving magma to the surface and into lateral dike systems, and hence for eruption rates. We anticipate using these results as guidelines in interpreting the locations, sizes and geometries of volcanic deposits.

References. [1] Ryan, M.P. (1987) p. 259 in Magmatic Processes: Physico-Chemical Prin-ciples. [2] Lister, J.R. (1990) JFM 210, 263. [3] Head, J.W. & Wilson, L. (1992) JGR 97, 3877. [4] Rubin, A.M. & Pollard, D.D. (1987) USGS Prof. Pap. 1350, 1449. [5] Wilson, L. & Head, J.W. (1983) Nature 302, 663. [6] Pollard, D.D. (1987) p.5 in Geol. Assoc. Can. Spec. Pap. 34. [7] Parfitt, E.A., Wilson, L. & Head, J.W. (1993) JVGR 55, 1.

Table 1. Crustal density (in kg m^{-3}) as a function of depth (in km) in basaltic volcanic areas on Earth and Mars, calculated using surface rock void fraction values discussed in the text, and densities of basaltic magmas containing 0.1 and 0.3 wt% CO_2 in their source zones. The underscore marks the neutral buoyancy level at which a magma reservoir is likely to be centred.

	Earth	Mars	magma		magma	
depth	crust	crust	0.1wt%		0.3wt%	
0	2200	1958	3	P	1	P
1	2364	2037	2442	N	2131	N
3	2600	2184	2571	N	2453	N
5	2739	2313	2597	N	2528	N
8	2840	2472	2600	N	2571	N
10	2868	2558	2600	N	2584	N
11	2877	2594	2600	N	2589	P
11.16	2878	2600	2600	-	2590	P
12	2884	2628	2600	P	2593	P
15	2894	2709	2600	P	2600	P